Structure of fumarate reductase from *Wolinella succinogenes* at 2.2 Å resolution

C. Roy D. Lancaster*, Achim Kröger†, Manfred Auer*‡ & Hartmut Michel*

* *Max-Planck-Institut für Biophysik, Heinrich-Hoffmann-Strasse 7, D-60528, Frankfurt am Main, Germany*
† *Johann Wolfgang Goethe-Universität, Institut für Mikrobiologie, Marie-Curie-Strasse 9, D-60439, Frankfurt am Main, Germany*
‡ *Present address: Skirball Institute of Biomolecular Medicine, NYU Medical Center, 540 First Avenue, New York, New York 10016, USA*

Fumarate reductase couples the reduction of fumarate to succinate to the oxidation of quinol to quinone, in a reaction opposite to that catalysed by the related complex II of the respiratory chain (succinate dehydrogenase). Here we describe the crystal structure at 2.2 Å resolution of the three protein subunits containing fumarate reductase from the anaerobic bacterium *Wolinella succinogenes*. Subunit A contains the site of fumarate reduction and a covalently bound flavin adenine dinucleotide prosthetic group. Subunit B contains three iron–sulphur centres. The menaquinol-oxidizing subunit C consists of five membrane-spanning, primarily helical segments and binds two haem *b* molecules. On the basis of the structure, we propose a pathway of electron transfer from the dihaem cytochrome *b* to the site of fumarate reduction and a mechanism of fumarate reduction. The relative orientations of the soluble and membrane-embedded subunits of succinate:quinone oxidoreductases appear to be unique.

Succinate dehydrogenases (succinate:quinone reductases, SQR) and fumarate reductases (quinol:fumarate reductases, QFR) catalyse the oxidation of succinate to fumarate as well as the reverse reaction. SQR (complex II) is involved in aerobic metabolism as part of the citric acid cycle and of the aerobic respiratory chain[1]. QFR is involved in a form of anaerobic respiration with fumarate as the terminal electron acceptor[2,3], and is part of the electron transport chain catalysing the oxidation of various donor substrates (such as NADH, H_2 or formate) by fumarate. These reactions are coupled by an electrochemical proton gradient to phosphorylation of ADP with inorganic phosphate by ATP synthase.

QFR and SQR complexes are collectively referred to as succinate:quinone oxidoreductases (EC 1.3.5.1) and are predicted to share similar structures. The complexes consist of two hydrophilic and one or two hydrophobic, membrane-integrated subunits[4]. The larger hydrophilic subunit A carries a covalently bound flavin adenine dinucleotide (FAD), and subunit B contains three iron–sulphur centres. QFR of *W. succinogenes* and SQR of *Bacillus subtilis*

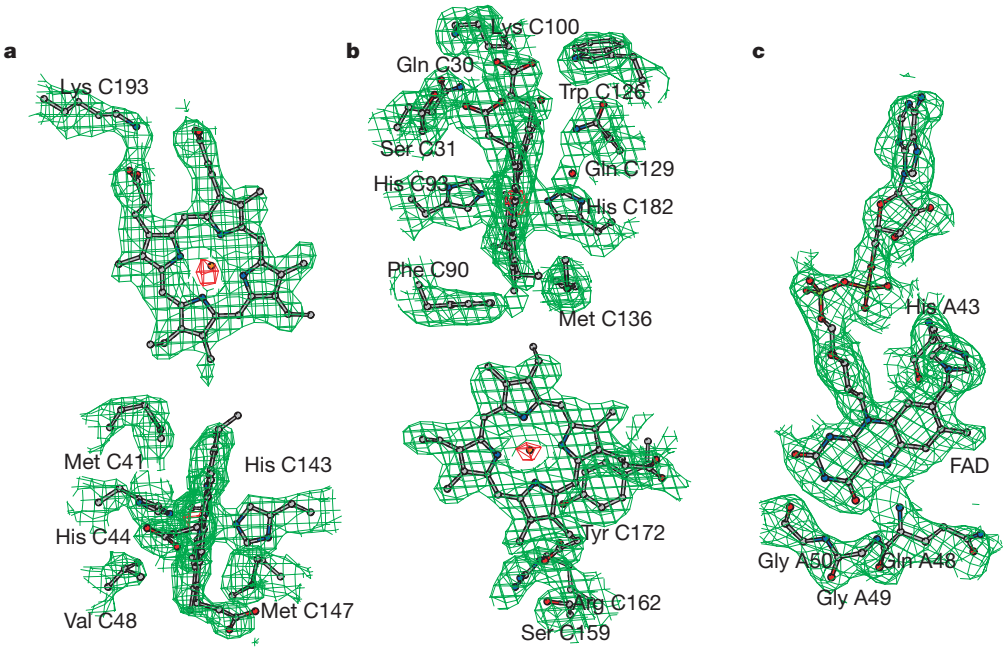

Figure 1 Representative parts of the experimental electron-density maps for crystal form A calculated with the MIRAS phases after density modification and phase extension to 2.2 Å resolution. C, N, O, P and S atoms are shown in grey, blue, red, light green and green, respectively; haem iron centres are shown in orange. Contour levels are 1.0 σ (green) and 9.0 σ (red) above the mean density of the map. Figs 1–4 and 6 were prepared with a version of Molscript[46] modified by R. Esnouf for colour ramping[47] and map drawing[48] capabilities. **a**, **b**, The two haem *b* molecules (b_P in the top half; b_D in the bottom half of each panel) and the side chains of some neighbouring residues in the transmembrane region. **c**, The covalently bound FAD prosthetic group.

contain only one hydrophobic subunit (C) with two haem *b* groups. In contrast, SQR and QFR of *Escherichia coli* contain two hydrophobic subunits (C and D) which bind either one (SQR) or no haem *b* group (QFR). Recently, the structure of this haem-free *E. coli* QFR has been described at a resolution of 3.3 Å (R_{free} = 29.2%; 49,332 unique reflections)[5].

We have determined at 2.2 Å resolution the structure of the *W. succinogenes* QFR containing two haem groups by X-ray crystallography. Here we describe the overall structure of the complex, the structures of the three subunits and the arrangement and binding mode of the six prosthetic groups. As a result, we propose a pathway of electron transfer and a mechanism of fumarate reduction. We also compare the structure with that of the *E. coli* enzyme. The relative orientations of the soluble and the membrane-embedded subunits differ between the two enzymes.

Structure determination

The fully oxidized fumarate reductase from *W. succinogenes* was crystallized (see Methods). Under these conditions we obtained crystals with two different unit cells, both belonging to space group $P2_1$. Crystal form 'A' has unit cell dimensions a = 85.2 Å, b = 189.0 Å, c = 117.9 Å and β = 104.5°. Crystal form 'B' has unit cell dimensions a = 118.4 Å, b = 85.1 Å, c = 188.9 Å and β = 96.5°. In both cases, there are two fumarate reductase complexes in the asymmetric unit. Data collection statistics and the quality of initial phases determined for crystal form A are summarized in Table S1 (see Supplementary Information). The phases were improved using a series of density-modification methods. Representative electron-density maps are shown in Fig. 1. The excellent quality of the experimental map allowed rapid model building for most of the structure. We then used the partially refined structural model for crystal form A (R = 26.5, R_{free} = 28%) as a search model for the phase determination of crystal form B by molecular replacement (see Supplementary Information). The refined structural models for crystal forms A (R = 21.2%, R_{free} = 22.4%; Table 1) and B (R = 21.3%, R_{free} = 22.3%) contain 2,296 of the 2,302 residues of the fumarate reductase dimer. Only the carboxy-terminal residue A656 of each A subunit and the two C-terminal residues C255 and C256 of each C subunit are not included. (Throughout this article, single letters in residue names refer to subunit identifiers, and amino-acid residues are represented by their three-letter codes.) For each asymmetric unit, two FAD groups, two Fe_2S_4, two Fe_4S_4 and two Fe_3S_4 iron–sulphur centres, and four haem *b* molecules, are included in the current models. The structures contain two metal cations and two dodecyl β-D-maltoside detergent molecules as well as 691 (form A) and 504 water molecules (form B), respectively. In addition, the structure for crystal form B also contains two fumarate molecules. The ratios of the number of independent observations to the number of parameters required to define the model, n_{obs}/n_{par} (Table 1), are 2.31 (form A) and 2.02 (form B). The corresponding value for the structure of *E. coli* fumarate reductase[5] is 0.73.

The experimental electron density (Fig. 1a–c) was of sufficiently high quality to identify a region of nine residues (Asp A281 to Pro A289) where the previously determined[6] sequence was incorrect. This has since been confirmed by resequencing (J. Simon and A.K., unpublished data).

Table 1 Refinement statistics

	Form A native	Form B native
Resolution range (Å)	38.63–2.20	38.87–2.33
No. of reflections used (completeness)	178,755 (98.0%)	152,939 (95.8%)
in working set	176,275 (96.6%)	150,440 (94.3%)
in test set	2,480 (1.4%)	2,499 (1.6%)
R_{free} (%) (38.63–2.33 Å)*	22.4 (22.0)	22.3
R_{cryst} (%) (38.63–2.33 Å)†	21.2 (20.8)	21.3
Luzzati coor. error (Å)‡	0.26 (0.28)	0.28 (0.30)
SIGMAA coor. error (Å)§	0.21 (0.21)	0.25 (0.25)
Highest resolution shell (Å)	2.25–2.20	2.39–2.33
$I/\sigma(I)$	2.9	2.8
Completeness	99.2%	99.7%
No. of non-hydrogen atoms in the model		
Atoms with occupancy >0	19,055	18,632
Average B-factor (Å^2)	32.5	39.0
No. of solvent molecules	691	504
n_{obs}/n_{par}‖	2.31	2.02
r.m.s. deviations from ideal values¶		
bond lengths (Å)	0.007	0.007
bond angles (°)	1.301	1.298
dihedral angles (°)	21.7	21.5
improper angles (°)	1.64	1.64
NCS r.m.s. difference (Å)	0.015	0.009

* R_{free} is the free R-value[40] calculated for the full resolution range and for the 38.63 to 2.33 Å range (in parentheses) = $\Sigma_{(hkl)\in T}||F_{obs}| - |F_{calc}||/\Sigma_{(hkl)\in T}|F_{obs}|$, where T is the test set (one reflection in each of at least 2,400 thin resolution shells[41] of the data).

† R is the crystallographic R-factor, calculated for the full resolution range of the working set and for the 38.63 to 2.33 Å range (in parenthesis) = $\Sigma_{(hkl)}||F_{obs}| - |F_{calc}||/\Sigma_{(hkl)}|F_{obs}|$.

‡ Estimate of the mean coordinate error from a Luzzati plot[42].

§ Estimate of the mean coordinate error from a SIGMAA plot[43].

‖ n_{obs}, number of observed unique reflections used in the working set; n_{par}, number of parameters necessary to define the model; this includes three parameters (x, y, z coordinates) per atom plus one (isotropic atomic B factor).

¶ Based on protein parameters files[44], haem cofactor parameter files[45] and parameter files generated for the other prosthetic groups and the substrate (see Supplementary Information).

Fumarate reductase architecture

In both crystal forms, the two fumarate reductase complexes in the asymmetric unit are associated in an identical fashion, forming a dimer. A view of the *W. succinogenes* fumarate reductase dimer parallel to the membrane is shown in Fig. 2a. In projection, as viewed in Fig. 2a, the part of the dimer that is integrated into the membrane has a trapezoidal appearance. It comprises ten membrane-spanning, primarily helical segments and their connections. These features of trapezoidal appearance and the smaller periplasmic surface as compared to the cytoplasmic surface resemble those of the structure of cytochrome *c* oxidase, complex IV of the respiratory chain[7]. The globular subunits B and A are attached to the trapezoid from the top. When viewed along the membrane normal, as in Fig. 2b, the membrane part of the fumarate reductase dimer is ellipsoidal.

About 3,665 Å^2 (8%) of the monomer surface is buried upon dimer formation. This is more than eleven times the value of ~325 Å^2 reported[5] for the *E. coli* fumarate reductase dimer, indicating that the dimer in the present structure is much more tightly associated. The portion of buried surface varies for the different subunits and is highest for the C subunit (12.2%). It is 2.6% for the A subunit and negligible for the B subunit. The dimer interface is mainly apolar, but 28% of the C subunit dimer interface is polar.

Protein subunits and prosthetic groups

The protein subunits are shown as Cα traces in Fig. 3a–d.

Subunit A. This subunit has a relative molecular mass of 73,000 (M_r = 73K)[6] and comprises four domains (Fig. 3a): a large FAD-binding domain (residues A1–260 and A366–436), a capping domain (A260–366), a helical domain (A436–554) consisting of a single helix and a three-helix bundle, and a C-terminal domain (A554–655), consisting of a pair of antiparallel β-strands followed by a longer and a short helix (Fig. 3a).

The FAD-binding domain with its Rossmann-type fold is structurally similar to some other FAD-binding proteins. The α-carbon atoms of the FAD-binding domain superimpose on those of thioredoxin reductase[8] with a root mean square (r.m.s.) deviation of 3.4 Å for 211 of the thioredoxin reductase residues, as determined using DALI[9].

Of the 655 Cα atoms in the model of the A subunit, 358 (54.7%) could be aligned (with an r.m.s. deviation of 1.7 Å) to a model containing 478 residues of *E. coli* L-aspartate oxidase (PDB entry 1CHU, provided before release by A. Mattevi[10]), with 109 residues (16.6% of the A subunit) found to be identical. The degree of similarity was higher for the FAD-binding domain and the three-

helix bundle of the helical domain and lower for the capping domain and the C-terminal domain. Subunit A of the structure of *E. coli* fumarate reductase can be superimposed on subunit A of the present structure with an r.m.s. deviation of 1.3 Å for 531 Cα atoms, illustrating the high degree of structural similarity for the first three domains of this subunit.

FAD binding. The A subunit of all described membrane-bound succinate:quinone oxidoreductase complexes contains a covalently bound FAD prosthetic group[11,12]. In *W. succinogenes* fumarate reductase, His A43 binds FAD by an 8α-[Nε-histidyl]-linkage to the isoalloxazine ring[13]. FAD is apparently further held in place by hydrogen bonds donated by the peptide NH groups of eleven residues (A13, A15, A16, A36, A44, A49, A50, A181, A393, A409 and A410) and the Oγ atoms of four Ser residues (A35, A42, A44 and A409). With the exception of residue A44, which is a Thr in most other succinate:quinone oxidoreductases, these Ser residues are highly conserved. The peptide CO group of residue A50 accepts a hydrogen bond from FAD (Fig. 1c). The flavin is also indirectly hydrogen-bonded through water molecules to the peptide NH groups of five residues (A14, A17, A43, A48 and A394) and to the peptide CO groups of residues A215, A216 and A319.

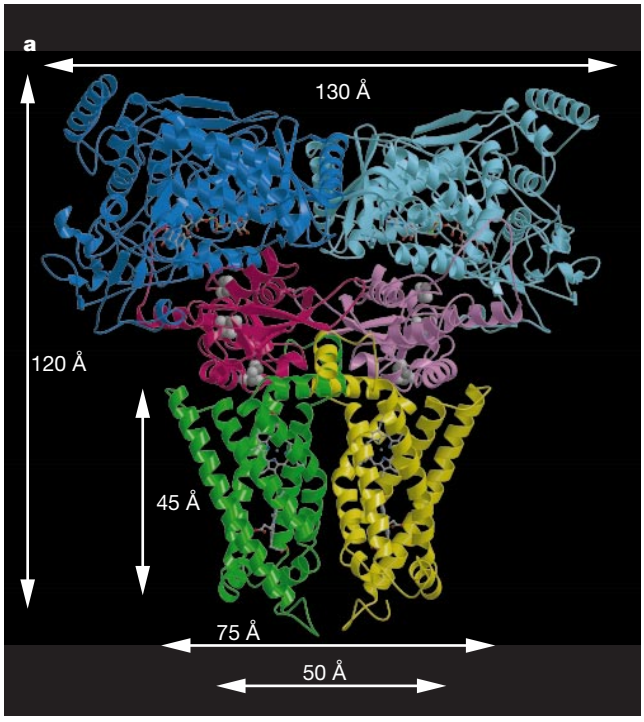

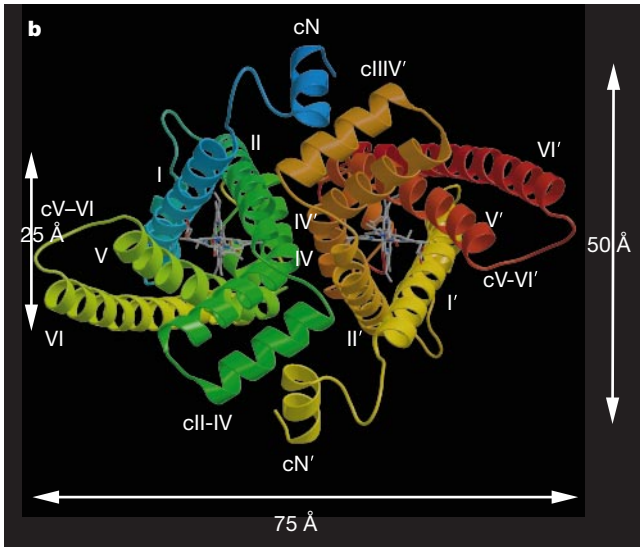

Figure 2 The three-dimensional structure of fumarate reductase. **a**, The fumarate reductase dimer viewed parallel to the membrane. The polypeptide backbones of the two A subunits are shown in blue and light blue, those of the two B subunits in red and pink, and those of the C subunits in green and yellow. Subunit A contains a covalently bound FAD. Subunit B contains three iron–sulphur clusters (Fe_2S_2, Fe_4S_4 and Fe_3S_4). The membrane-embedded subunit C contains two haem *b* molecules. **b**, View of the transmembrane helices of the subunit C dimer along the membrane normal from the cytoplasmic side. One monomer is colour-coded from blue (N terminus) to yellow (C terminus), the other from yellow (N terminus) to red (C terminus)). The transmembrane helices are labelled I, II, IV, V and VI (ref. 22). Secondary structures were assigned using DSSP[49]. Figure rendered with Raster3D[50].

A new metal-binding site. During refinement, we identified an apparent additional metal-binding site. It is located in the FAD-binding domain of subunit A, less than 8 Å from the FAD group and less than 12 Å from its isoalloxazine ring system. Five backbone carbonyl oxygens (A371, A372, A373, A393, A395) as well as one tightly bound water molecule are involved in the binding of this metal cation of unknown function. In the refined models, it has been tentatively assigned to be a Ca^{2+} ion.

The dicarboxylate site. The data set of crystal form B is based on a crystal grown in the presence of 1 mM fumarate instead of 1 mM malonate. In the refined structure, we found significant difference density corresponding in shape to a fumarate molecule close to the isoalloxazine ring of FAD (Fig. 4a). Apparently, the dicarboxylate-binding site is mainly formed by the isoalloxazine ring of FAD, two arginine side chains (Arg A301 and Arg A404), one histidine side chain (His A369; Fig. 4b) and the side chain of Phe A141 (not shown in Fig. 4). One carboxylate group of fumarate is bound by polar interactions with Arg A404 and His A369, the other by Arg A301.

As viewed in Fig. 4, the left carboxyl group of the fumarate molecule is distorted. Its oxygen atoms are out of plane with respect to the rest of the fumarate molecule. Quantum chemical calculations at the MP2/6-31G* level (M. Hutter & C.R.D.L., unpublished data) indicate that the energy required to distort the molecule is 4.6 kcal mol^{-1}. This could be accounted for by one additional hydrogen bond, which can be donated by His A369. For an idealized planar fumarate molecule, the closest carboxyl oxygen would be ~0.9 Å further away from this residue. In addition, based on the position of the rest of the molecule, binding of an idealized planar fumarate would not be favoured owing to unfavourable steric interactions of the left carboxyl group with the FAD isoalloxazine ring.

If the imidazole ring of His A257 (not shown) were to be flipped by 180° around the χ_2 torsional angle, its Nε atom would be within hydrogen-bonding distance of the fumarate γ-carboxylate. However, this flip would also lead to possibly unfavourable interactions of the Nε atom with the guanidino group of Arg A301 and of the Nδ atom with the peptide NH of Thr A259. Also, the hydrogen bond donated by the Nε atom to the Oγ of Thr A259 would be lost. Therefore, the orientation of His A257 as included in the model is determined by its arrangement within the conserved 'HPT triad' of His A257, Pro A258 and Thr A259.

Tightly bound by hydrogen bonds from both Arg A301 and Arg A404, there is a water molecule, which is also within hydrogen-bonding distance of the fumarate α-methenyl C atom. Within hydrogen-bonding distance of the fumarate β-methenyl C atom, there is a second water molecule (Fig. 4a) which is also within hydrogen-bonding distance of N5 of the FAD isoalloxazine ring and the peptide NH of A48. The side chain Oγ atom of Ser A409 is in a position to form hydrogen bonds with the N1 and O2 atoms of the FAD isoalloxazine ring and the guanidino group of Arg A404. All residues shown in Fig. 4 are widely conserved among succinate:quinone oxidoreductases.

Whereas the proximity of two Arg side chains and of FAD to the dicarboxylate binding site was expected[14], the location of the Arg side chains in the sequence and the presence of His A369 at the

binding site were less obvious. Particularly unexpected is the finding that Arg A273, which is homologous to Arg A248 of *E. coli* fumarate reductase, is absent from the inner shell of residues at the active site. For the *E. coli* enzyme, this residue was deduced by site-directed mutagenesis to be directly involved in substrate binding[15]. In the *W. succinogenes* enzyme, Arg A273 is located in a segment containing four conserved Gly residues (A271, A274, A276 and A277). In the structure, the Arg side chain is oriented away from the dicarboxylate site. Mutation of this residue apparently has larger structural consequences.

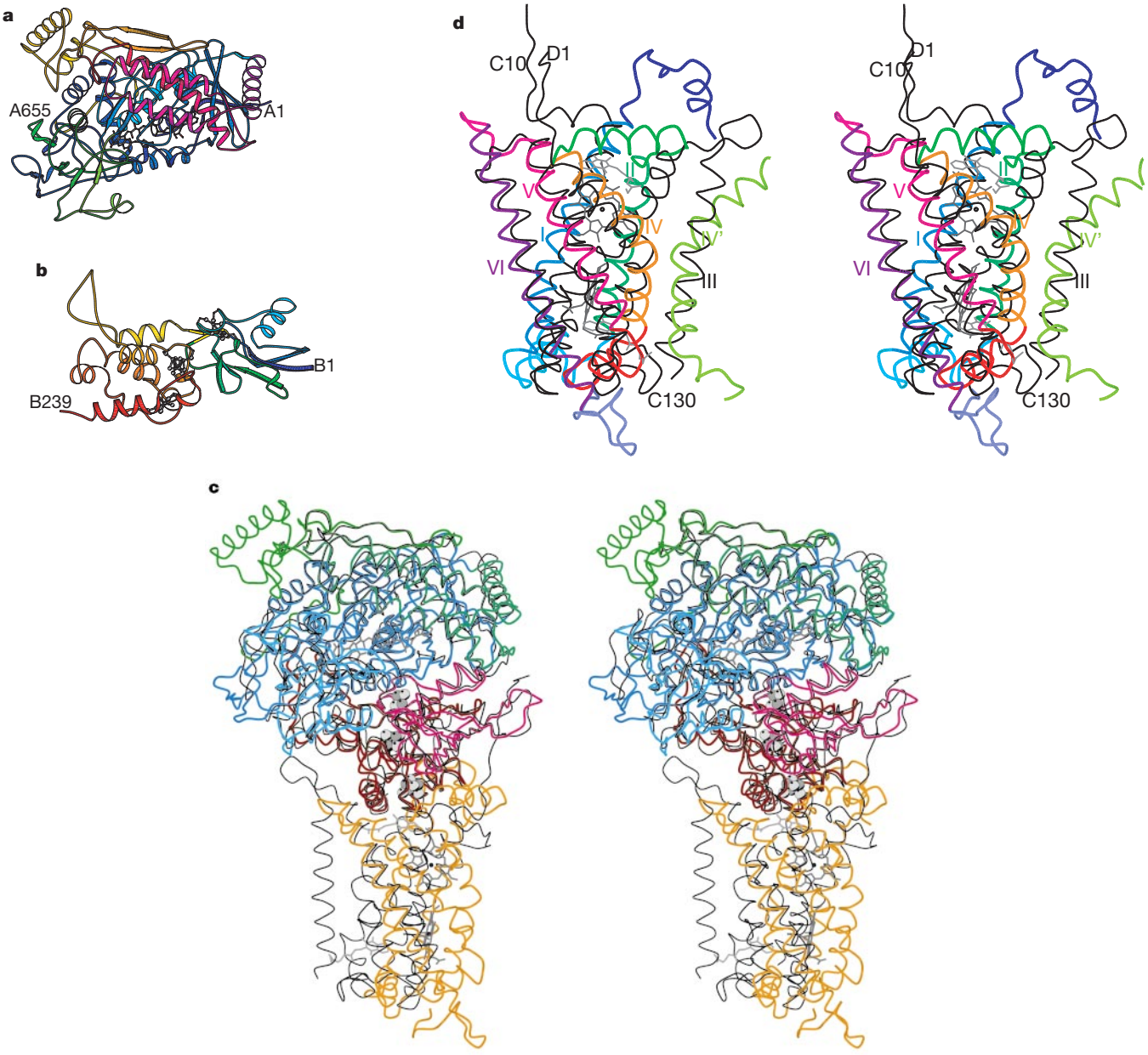

Figure 3 Structure of the subunits of *W. succinogenes* fumarate reductase. The structure of *E. coli* fumarate reductase[5] is shown in black in **c** and **d** for comparison. The prosthetic groups FAD, haem b_P and haem b_D of the *W. succinogenes* enzyme are drawn as stick models and the iron–sulphur centres as grey spheres. The quinone models of the *E. coli* enzyme are in grey. **a**, *W. succinogenes* subunit A. Residues A1–260 and A366–436 constitute the FAD-binding domain (colour-coded from dark blue to light blue by sequence); A260–366 form the capping domain (dark green to light green); and A436–554 constitute the helical domain (purple to red) with a single helix (A437–456) followed by a three-helix bundle (A463–477, A484–501, A515–539). The C-terminal domain (A554–655, orange to yellow) includes an antiparallel pair of β-strands (A562–567, A577–582) followed by a longer (A607–625) and a short (A730–637) helix. **b**, *W. succinogenes* subunit B. The N-terminal plant ferredoxin domain (B1–98, colour-coded from blue (N terminus) to green (C-terminal end of domain)) consists of a pair of antiparallel β-strands (B4–11 and B22–29), followed by a helix (B36–46) which precedes the Cys residues (B57, B62, B65 and B77), which are ligands to the Fe_2S_2 iron–sulphur centre. The C-terminal bacterial ferredoxin domain (B98–239, yellow (N-terminal) to red (C-terminus) consists of five helices, two preceding (B108–117 and B139–148) the first cluster of Cys residues (B151, B154, B157 and B161) and another two preceding the second cluster of Cys residues (B208, B214 and B218), followed by a C-terminal helix (B224–235). **c**, Stereo view. *W. succinogenes* subunit A domains in blue (FAD-binding domain), light blue (capping domain), blue-green (helical domain) and green (C-terminal domain) as in **a**. Subunit B domains in pink (plant ferredoxin domain) and brown (bacterial ferredoxin domain) as in **b**. Subunit C is orange. **d**, Stereo view. *W. succinogenes* subunit C consists of five transmembrane helices, two periplasmic and two cytoplasmic helices. The N-terminal cytoplasmic helix (dark blue) is followed by transmembrane helix (TH) I (blue), a short periplasmic helix (light blue), TH II (blue-green), a second cytoplasmic helix (green), TH IV[22] (orange), which is strongly kinked at position C137, a second periplasmic helix (red), TH V (pink) and TH VI (purple). Haem b_P (top half) and haem b_D (bottom half) are dark grey.

The side chain of residue Cys A272, proposed[6] to be the site of inhibition by sulphydryl reagents[16] such as pCMS (4-chloromercuriphenylsulphonate), is disordered and was not found to be labelled by pCMB (see Supplementary Information) or pCMS (C.R.D.L. & H.M., unpublished data). Instead, these reagents labelled residue Cys A6 which, in the 22 most related sequences, is only conserved in the fumarate reductase of *Helicobacter pylori*[17] and in the L-aspartate oxidase of *E. coli*[18].

Chemistry of fumarate reduction. The arrangement of residues forming the active site of the oxidized enzyme with fumarate (Fig. 4a) suggests a mechanism of fumarate reduction as outlined in Fig. 5: $FADH_2$ presumably donates a hydride ion from its N5 to the β-methenyl group of fumarate. This hydride transfer could occur directly (Fig. 5a). In synchrony with this process, two of the double-bond electrons of fumarate move toward the α-carbon, and not the positively charged imidazolium group of His A257 (as proposed in ref. 19), but the tightly-bound water molecule donates a proton to the α-methenyl group to stabilize the reduced substrate. This proton could then be replenished by transfer via Ser A409 and Arg A404 of the proton released at the N1 position upon oxidation of $FADH_2$ (Fig. 5b). The water molecule within hydrogen-bonding distance of the FAD N5 and the Ser Oγ atom within hydrogen-bonding distance of the FAD N1 are likely to be involved in the reorientation of hydrogen bonds upon oxidation of $FADH_2$. Release of the product could be facilitated by domain movement of the capping domain, thus moving residue Arg A301 away from the dicarboxylate site (Fig. 4b).

Subunit B. This subunit (M_r = 27K)[6] consists of two domains, an amino-terminal 'plant ferredoxin' domain (B1–98, Fig. 3b), binding the Fe_2S_2 iron–sulphur centre, and a C-terminal 'bacterial ferredoxin' domain (B98–239) binding the Fe_4S_4 and the Fe_3S_4 iron–sulphur centres, as was expected from sequence comparisons[6]. The α-carbon atoms of the plant ferredoxin domain superimpose on Fe_2S_2-ferredoxin[20] with an r.m.s. difference of 2.0 Å for 64 of the 96 Fe_2S_2-ferredoxin residues.

Although the homology to bacterial Fe_4S_4-ferredoxins of the sequence in the ligand-binding segments of the bacterial ferredoxin domain has been pointed out[6,4], no superposition of coordinates with DALI was possible. The fragments containing ligands of the Fe_3S_4 and Fe_4S_4 centres are inverted in sequence with respect to bacterial ferredoxins containing Fe_3S_4 and Fe_4S_4 centres. With an r.m.s. deviation of 1.4 Å, 222 Cα atoms of subunit B from *E. coli* fumarate reductase[5] can be superimposed onto those of the present coordinates (Fig. 3c), indicating that this subunit is structurally very similar in both enzymes.

More than one-third of the surface area of subunit B is buried upon formation of the fumarate reductase ABC monomer, with 22% of the surface buried by subunit A and 12% of the subunit B surface buried by subunit C.

Iron–sulphur centres. The Fe_2S_2 iron–sulphur centre is coordinated by Cys residues B57, B62, B65 and B77, as proposed on the basis of sequence alignments[6]. All four Cys residues are within segments that are in contact with the A subunit. For instance, the peptide CO of Cys B62 is hydrogen-bonded to the guanidino group of Arg A41, which is close to the point of covalent FAD attachment. The Fe_4S_4 iron–sulphur centre is ligated to the protein through Cys residues B151, B154, B157 and B218, and the Fe_3S_4 centre is coordinated by Cys residues B161, B208 and B214 (Fig. 3b). The last three residues

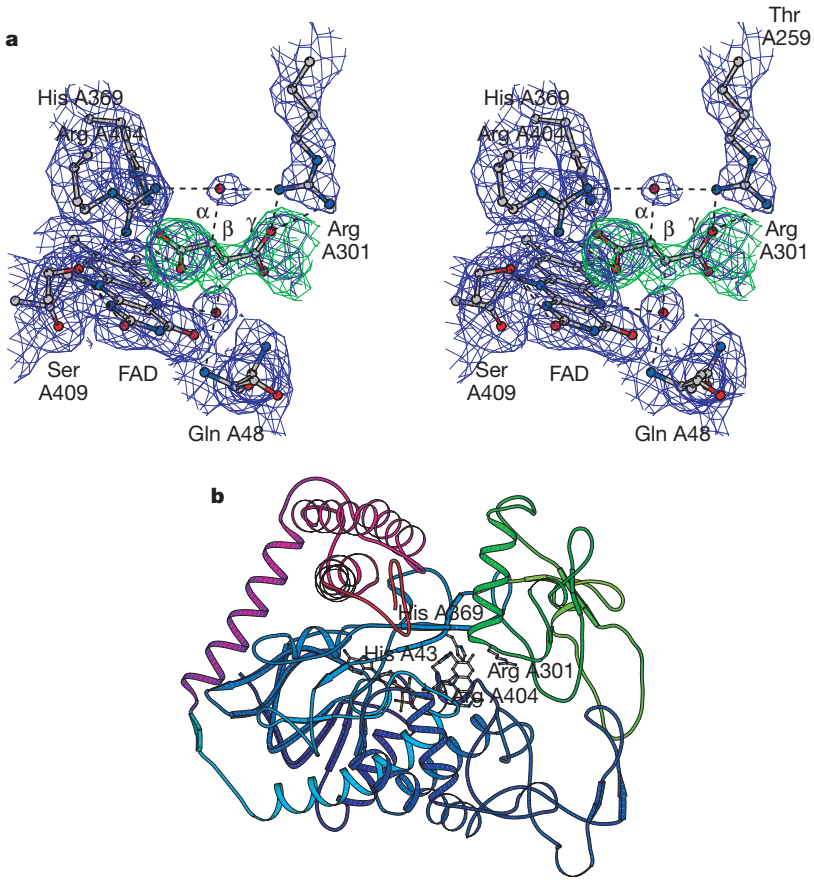

Figure 4 The dicarboxylate binding site in subunit A. **a**, Stereo view. SIGMAA-weighted electron-density maps form the refined model of crystal form B at 2.33 Å resolution. Contour levels are 1.0 σ ($2mF_o - DF_c$, purple) and 3.0 σ ($mF_o - DF_c$, green, with the fumarate molecule omitted from the phase calculation). Distances compatible with hydrogen-bonding and salt-bridge interactions are indicated by dashed lines. Also labelled are the α- and β-methenyl and γ-carboxylate groups of fumarate (see text). **b**, Alternative view of the first three domains of subunit A, colour coded as in Fig. 3a, with the three residues Arg A301, His A369 and Arg A404 lining the binding site shown.

are within segments that are in contact with the C subunit.

Subunit C. This subunit (M_r = 30K)[21] contains five membrane-spanning segments with preferentially helical secondary structures (Fig. 3d). These segments are labelled (according to ref. 22) I (C22–52), II (C77–100), IV (C121–149), V (C169–194) and VI (C202–237). According to the alignment of ref. 22, there is no transmembrane segment III in *W. succinogenes* fumarate reductase. To a varying degree, all five transmembrane segments are tilted with respect to the membrane normal. When viewed from the cytoplasmic side (Fig. 2b), the first four transmembrane segments appear to form a pore-like structure. The 'pore' is blocked by haems b_P and b_D (Fig. 2b). This is different from the haem arrangement in cytochrome *c* oxidase, where the membrane-bound haem molecules block two different pores[7]. The membrane-spanning segments are connected by four loops referred to as C-subunit loops pI–II, cII–IV, pIV–V and cV–VI, with c and p denoting loops on the cytoplasmic and periplasmic side of the membrane, respectively. Three of these loops contain short helices (pI–II: C55–63; cII–IV: C105–118; pIV–V: C158–164). The N terminus of subunit C is on the cytoplasmic side and the C terminus on the periplasmic side of the membrane. The N-terminal residues C3–11 form a helix denoted 'cN'. The C-terminal residues C237–254 are of extended secondary structure with turns, and form the bottom of the C subunit. Residues C255 and C256 are disordered and are not visible in the electron-density map.

About one-tenth (9.7%) of the surface of subunit C is buried by forming contacts with subunit B. About one-eighth (12.2%) of the surface of subunit C is buried by interactions with the second subunit C molecule in the fumarate reductase dimer.

Haems b_P and b_D. Unlike the fumarate reductase of *E. coli*, which does not contain any haem groups, and the succinate dehydrogenase of *E. coli*, which contains one haem *b*, the C subunit of the *W. succinogenes* enzyme is a dihaem cytochrome *b*[21]. The planes of both haem molecules are approximately perpendicular to the membrane surface and their interplanar angle is 95° (Figs 1, 2b).

The axial ligands to the 'proximal' haem b_P are His C93 of transmembrane segment II and His C182 of transmembrane segment V (Fig. 1b). This causes haem b_P to be located towards the cytoplasmic surface of the membrane, and thus towards the Fe_3S_4 iron–sulphur centre. Hydrogen bonds and salt bridges with the propionate groups of haem b_P are formed with the side chains of residues Gln C30, Ser C31, Lys C100, Trp C126 (Fig. 1b) and Lys C193 (Fig. 1a). Thus, side chains from the residues of all four transmembrane segments forming the pore described above are involved in the binding of haem b_P, underscoring the structural importance of the bound haem[23].

The axial ligands to the 'distal' haem b_D are His C44 of transmembrane segment I and His C143 of transmembrane segment IV (Fig. 1a), showing that all four haem axial ligands had been correctly predicted by sequence alignment[21] and site-directed mutagenesis[23]. Hydrogen bonds to the ring A propionate can be donated by the side chains of Ser C159 and Tyr C172, and a salt bridge with the Arg C162 side chain is possible (Fig. 1b). No such interactions can be found for the ring D propionate of haem b_D.

The binding of the two haem *b* molecules described here is very different from that described for the cytochrome bc_1 complex[24]. In *W. succinogenes* fumarate reductase, the axial ligands for haem binding are located on four different transmembrane segments. In the cytochrome bc_1 complex, only two transmembrane segments are involved, each providing two axial haem *b* ligands. One consequence of this difference is that the distance between the two haem iron centres is distinctly shorter in fumarate reductase (15.6 Å) than it is in the cytochrome bc_1 complex (21 Å).

Relative orientation of soluble and membrane-embedded subunits. As discussed above for the individual soluble subunits, the structure of *E. coli* fumarate reductase can be superimposed on the present structure with an r.m.s. deviation of 1.4 Å for 757 Cα atoms

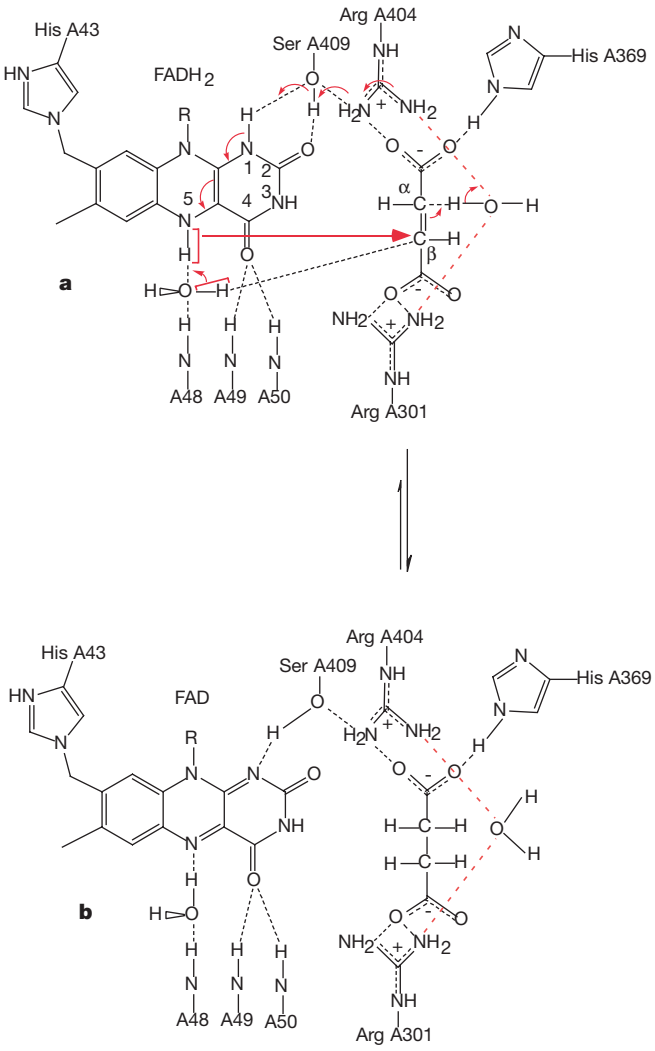

Figure 5 Possible mechanism of fumarate reduction in *W. succinogenes* fumarate reductase involving the residues shown in Fig. 4. In addition, the peptide backbone NH groups of residues A48–50 (Fig. 1c) are indicated. For clarity, only the isoalloxazine ring portion of FAD(H_2) is shown. Direct hydride ion transfer from the N5 of the $FADH_2$ isoalloxazine ring system (see Fig. 4) to fumarate is accompanied by proton transfer from the $FADH_2$ N1 position via a chain of hydrogen bonds, thus forming succinate.

from subunits A and B (Fig. 3c). This similarity in structure was expected on the basis of sequence comparisons. However, in this superimposition, the membrane-embedded subunits cannot be aligned. In an alternate superimposition, transmembrane subunits C and D of the *E. coli* enzyme can be overlayed onto the *W. succinogenes* C subunit with an r.m.s. deviation of 2.25 Å for 113 Cα atoms from transmembrane helices I, II, IV, V and VI, and from the two periplasmic helices pI–II and pIV–V (Fig. 3d). Compared to the former superimposition (Fig. 3c), the latter (Fig. 3d) involves a rotation around the membrane normal of approximately 180° and a 25° rotation in the plane of the paper. This leads to two important conclusions. First, the structures of the transmembrane subunits carrying no haems and two haems, respectively, can be aligned to a significant degree, although only eleven of the aligned residues are identical. Second, the relative orientation of the soluble subunits and the transmembrane subunits is different in the fumarate reductase complexes from the two species.

The superimposition shown in Fig. 3d can be extended to 172 Cα positions with a higher r.m.s. deviation of 3.0 Å. This increase is because the four transmembrane helices forming the pore shown in Fig. 2b are closer together in the haem-less *E. coli* enzyme than in

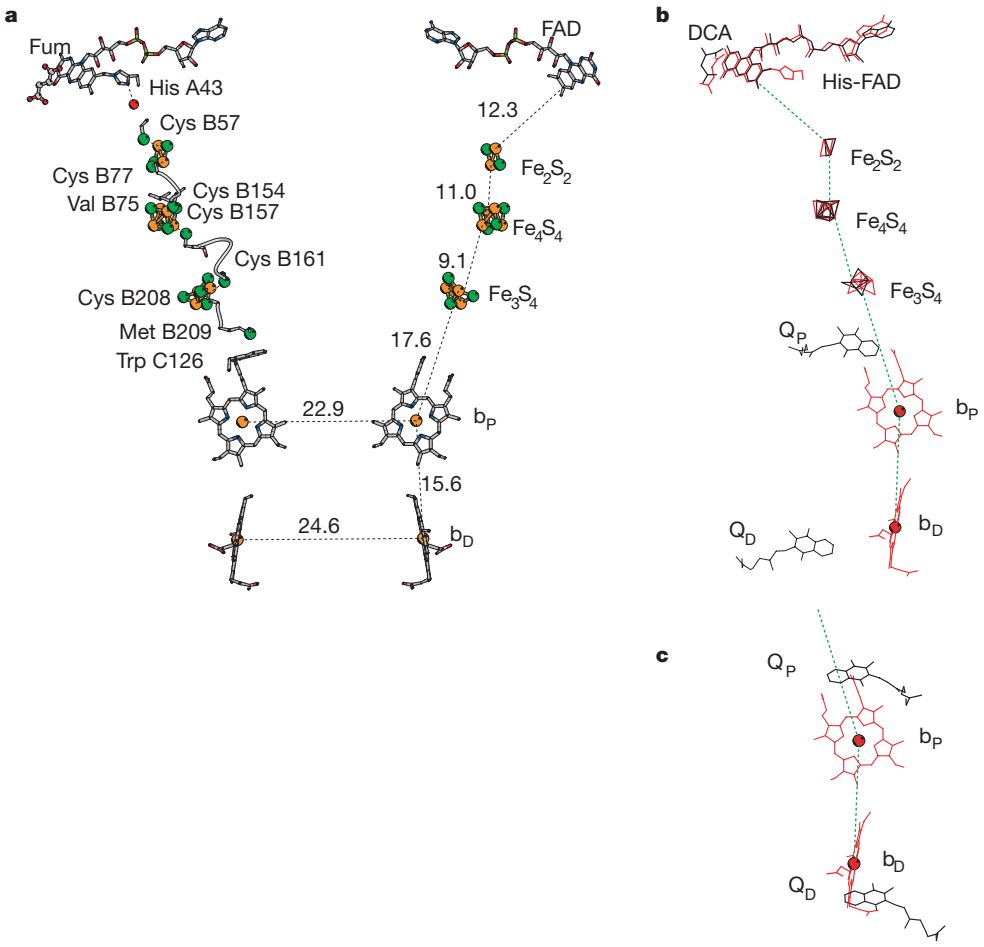

Figure 6 Arrangement of the prosthetic groups in the fumarate reductase dimer and possible electron-transfer pathways, including the position of bound fumarate (Fum). **a**, view as in Fig. 2a, colour coding as in Fig. 1. Numbers refer to indicated distances in Å. The side chain of Trp C126 is in a position to donate its hydrogen bond to the ring A propionate of haem b_P. This Trp side chain is in van der Waals contact (3.9 Å) with the Sδ of Met B209, which in turn is connected by the polypeptide backbone with Cys B208, a ligand to the Fe_3S_4 iron–sulphur centre. Another ligand of the Fe_3S_4 centre, Cys B161, is connected, both by the polypeptide backbone and by a hydrogen bond, to Cys B157, a ligand of the Fe_4S_4 centre. Similarly, the third ligand of the Fe_3S_4 centre, Cys B214, is connected to the second ligand of the Fe_4S_4 centre, Cys B218 (not shown). A third ligand of the Fe_4S_4 centre, Cys B154, is in van der Waals contact with Leu B75, which in turn is connected by the polypeptide backbone to Cys B77, a ligand to the Fe_2S_2 centre. A second ligand of the Fe_2S_2 centre is in van der Waals contact with a water molecule which is hydrogen-bonded to the Nδ atom of His A43, the site of covalent attachment of FAD. **b**, **c**, Comparison of the electron-transfer pathways in the fumarate reductase complexes of *W. succinogenes* (red) and *E. coli*[5] (black). Q_P, proximal quinone; Q_D, distal quinone. **b**, Structures are superimposed based on the Cα atoms of the A and B subunits (Fig. 3c). DCA, dicarboxylate (fumarate in the case of the *W. succinogenes* QFR coordinates (red) and oxaloacetate for the *E. coli* QFR coordinates (black)). **c**, Structures are superimposed based on the Cα atoms of the transmembrane subunits (Fig. 3d).

W. succinogenes fumarate reductase. For example, the distances between the Cα atoms of the *W. succinogenes* haem axial ligands are 13.0 Å (His C44–His C143) and 12.7 Å (His C93–His C182) for haems b_D and b_P, respectively. The corresponding distances in the *E. coli* enzyme are 9.9 Å (Leu C42–Met D31) and 11.2 Å (His C82–Cys D77). Another feature compensating for the absence of haems in the *E. coli* enzyme is the presence of more bulky residues (such as Arg C28, Trp C86 and Arg D81) where the corresponding positions in the *W. succinogenes* enzyme are occupied by smaller residues (Gln C30, Ala C97 and Gly C186). The superposition shown in Fig. 3d also indicates that the position of transmembrane helix III in the *E. coli* enzyme is occupied by transmembrane helix IV of the other *W. succinogenes* fumarate reductase monomer in the dimer. As the transmembrane subunit provides the largest contact area for the formation of the *W. succinogenes* QFR dimer, this superposition also explains the different degree of dimerization and different orientation of the monomers in the enzyme dimers of the two species.

Electron-transfer pathways

For fumarate reductase to function, electrons have to be transferred from the quinol-oxidizing site in the membrane to the fumarate-reducing site, protruding about 40 Å into the cytoplasm. For *W. succinogenes* fumarate reductase, the experimental data[25] are consistent with this electron transfer from the quinol to fumarate occurring through (at least) one haem *b* group. The shortest distance between haem b_P and haem b_D is 4.2 Å. This distance is even shorter than that between haem *a* and haem a_3 in cytochrome *c* oxidase[7], indicating that both haem *b* groups may be involved in electron transfer. In the event of transmembrane electron transfer via the haems, and if a 'distal' and a 'proximal' quinone-binding site are present (see below), electrogenic proton transfer, similar to the cytochrome bc_1 complex, is possible. This possibility awaits experimental verification.

The arrangement of the prosthetic groups in the fumarate reductase dimer is shown in Fig. 6a. As shown in Fig. 4, the fumarate molecule is in van der Waals contact with the isoalloxazine ring of FAD. The connectivity pattern shown in Fig. 6a therefore provides one straightforward pathway by which electrons could be transferred efficiently from the dihaem cytochrome *b* to the dicarboxylate-binding site.

The Fe_4S_4 iron–sulphur centre has a very low potential ($E_m = -250$ mV) and has been suggested not to participate in

electron transfer[4]. However, the determined low potential may be an artefact due to anti-cooperative electrostatic interactions between the redox centres[26]. The position of the Fe_4S_4 centre as revealed in the structure presented here is highly suggestive of a direct role in electron transfer from the Fe_3S_4 centre to the Fe_2S_2 centre.

The prosthetic groups of *W. succinogenes* fumarate reductase are compared with those of the *E. coli* enzyme on the basis of the superposition of the soluble subunits (Fig. 6b) and the superposition of the membrane-embedded subunits (Fig. 6c). Correlated with the similarity in structure of the soluble protein subunits (Fig. 3c, above), the histidyl–FAD group and the three iron–sulphur centres superimpose well, with the exception of those Fe_3S_4 sulphur atoms that are oriented towards the membrane-embedded subunit(s).

Quinone-binding sites. The existence of up to three quinone-binding sites in succinate:quinone oxidoreductases is being discussed[4]: a 'proximal' binding site, close to haem b_P (where present) and the Fe_3S_4 iron–sulphur centre, and a 'distal' binding site close to haem b_D. In some cases, the proximal binding site has been reported to contain an EPR-detectable semiquinone pair[4]. Although dimethylnaphthoquinone was present in the crystallization droplets, no density for a quinone could be found in either crystal form of the oxidized enzyme presented here. By analogy with the cytochrome bc_1 complex[24], the quinone-binding site(s) is (are) expected to be located in the vicinity of haem b_P (and haem b_D). By analogy to the photosynthetic reaction centre[27], the quinone(s) is (are) expected to bind in the vicinity of the Trp 'belts' in the hydrophobic surface-to-polar transition zone of the membrane (not shown).

The *E. coli* fumarate reductase coordinate set 1FUM (ref. 5) contains models for two quinone molecules per ABCD monomer. Although some of the B values of the quinone ring atoms are larger than 100 Å^2, indicating that these quinone models may not be well defined, these models have been included in Fig. 6b and c for comparison. In the superposition of the transmembrane subunits (Fig. 6c), the proximal quinone clashes with the ring A haem b_P propionate (Fig. 1b). The distal quinone clashes with the A haem b_D propionate. In summary, this superposition indicates that the quinone-binding site(s) of the two enzymes are not simply superimposable. In the *W. succinogenes* enzyme, they may be close to the haem molecules and the Trp belts, as previously inferred by comparison with other quinone-binding membrane proteins above. Note that quinones are the products and not the substrates of fumarate reductases. Therefore, binding of quinones might lead to substrate inhibition and has to be avoided. With this argument, the two quinones in the *E. coli* enzyme would have to be considered as structural quinones, with possible electron-transfer activities at least for the proximal quinone, and the existence of an additional quinol-binding site is required.

It is unlikely that transmembrane electron transfer occurs in the *E. coli* enzyme, because of the large gap of 27 Å between the two quinones. The close proximity between the two haems of *W. succinogenes* fumarate reductase as described above, however, offers a much more straightforward possibility for transmembrane electron transfer.

Conclusions

Most members of the succinate:quinone oxidoreductase superfamily contain at least one haem bound to the membrane-embedded subunit(s)[28]. The well refined structure of the fumarate reductase presented here is the first of a haem-containing succinate:quinone oxidoreductase. At 2.20 Å resolution, it is currently the highest resolution structure available of a respiratory membrane protein complex. In this structure, the arrangement of two haems in the transmembrane domain is revealed. This arrangement suggests an efficient pathway for transmembrane electron transfer. The high resolution (2.33 Å) of the structure with bound fumarate allows us to propose a catalytic mechanism for the reduction of fumarate to succinate. As all of the identified residues are conserved, this mechanism is of general relevance to all succinate:quinone oxidoreductases. In summary, the structure provides a framework for understanding the mechanism of complex II of the respiratory chain and related proteins at an atomic level. □

Methods

Enzyme purification and crystallization

W. succinogenes was grown with formate and fumarate as described[29]. Fumarate reductase was purified as described[30], except that the hydroxyapatite column was replaced by a DEAE CL-6B column and the detergent Triton X-100 was replaced by a mixture of dodecyl-β-D-maltoside/decyl-β-D-maltoside on a second DEAE CL-6B column. The enzyme was then subjected to isoelectric focusing. We used the preparative flat-bed electrofocusing procedure for the preparation of photosystem I (ref. 31) with the following modifications: the pH range of the ampholytes was 5–8 (servalyt 5–8), and dodecyl-β-D-maltoside (0.05%) and decyl-β-D-maltoside (0.20%) were added to the ampholine solution. The gel band containing fumarate reductase was cut out and suspended in a buffer (pH 7.3) containing 20 mM HEPES, 1 mM EDTA and 2 mM malonate. After sedimentation of the gel material by centrifugation, the ampholytes were removed by gel filtration on PD-10 columns (Pharmacia).

The fully oxidized fumarate reductase from *W. succinogenes* was crystallized in the presence of 1 mM $K_3Fe(CN)_6$, 0.05% dodecyl-β-D-maltoside, 0.20% decylmaltoside, 2.4% benzamidine, 5% polyethylene glycol (PEG-3350), 75 mM NaCl, 5% dimethylformamide (DMF), 1 mM dimethylnaphthoquinone (DMN), 1 mM malonate and 10 mM HEPES/10 mM citrate, pH 6.4, at a protein concentration of 9.5 mg ml^{-1} by vapour diffusion against a reservoir containing 150 mM NaCl, 10% PEG-3350 and 20 mM citrate, pH 5.6. Nucleation was enhanced by applying the microseeding technique[32].

Diffraction data

X-ray data were collected at ESRF beamline BM14 ($\lambda = 0.996$ Å, $T = 2$–4 °C), Grenoble. Owing to their thickness, the redox state of the crystals could not be monitored *in situ*. Intensity data were obtained using a CCD detector (MAR). Additional data were collected in-house with a rotating anode X-ray generator as source (CuKα, $\lambda = 1.5418$ Å) and an R-Axis IIC imaging plate as detector. Only one crystal was required for each dataset listed in Table S1 (see Supplementary Information). Data were processed with the HKL programs DENZO and SCALEPACK[33].

Phasing

Heavy-atom sites were determined from difference Patterson maps. The relative positioning of sites between derivatives was determined by the difference Fourier technique, using series of programs in the CCP4 suite[34]. MIRAS (multiple isomorphous replacement with anomalous scattering) phasing and refinement of the heavy-atom positions were initially done using SHARP[35]. Iron positions were determined iteratively from a consistent set of peaks in the SHARP anomalous residual maps of the native and derivative data sets, which were absent in the isomorphous residual maps. After inclusion of all 22 Fe sites in the asymmetric unit for all data sets, phase calculation and refinement was completed with MLPHARE[36].

Density modification

Density modification and phase extension to 2.20 Å were performed with the program DM[37]. Solvent flattening using a solvent content of 60%, histogram matching and averaging were applied using the initial non-crystallographic symmetry (NCS) operator determined from the heavy atom and iron positions. Phase extension was performed in resolution steps, starting with the low-resolution data (50-5 Å), where the figure of merit was high. The initial real-space R value was 0.258, but it was reduced to 0.116 after 100 cycles, and the NCS correlation between regions of related density increased from 0.676 to 0.919.

Model building and refinement

The atomic model of fumarate reductase was built using program O[38]. Simulated annealing, followed by conventional positional refinement and restrained individual B-factor refinement, was performed using CNS[39]. Initially, strict NCS constraints were applied between the two fumarate reductase monomers in the asymmetric unit. In later cycles of refinement these were replaced by NCS restraints with a weight of 300 kcal mol^{-1} Å^{-2}.

Received 23 June; accepted 14 October 1999.

1. Saraste, M. Oxidative phosphorylation at the fin de siècle. *Science* **283,** 1488–1493 (1999).
2. Kröger, A. Fumarate as terminal acceptor of phosphorylative electron transport. *Biochim. Biophys. Acta* **505,** 129–145 (1978).
3. Kröger, A. *et al.* Bacterial fumarate respiration. *Arch. Microbiol.* **158**, 311–314 (1992).
4. Hägerhäll, C. Succinate:quinone oxidoreductases. Variations on a conserved theme. *Biochim. Biophys. Acta* **1320,** 107–141 (1997).
5. Iverson, T. M., Luna-Chavez, C., Cecchini, G. & Rees, D. C. Structure of the *Escherichia coli* fumarate reductase respiratory complex. *Science* **284,** 1961–1966 (1999).

6. Lauterbach, F. *et al.* The fumarate reductase operon of *Wolinella succinogenes*. Sequence and expression of the frdA and frdB genes. *Arch. Microbiol.* **154,** 386–393 (1990).
7. Iwata, S., Ostermeier, C., Ludwig, B. & Michel, H. Structure at 2.8 Å resolution of cytochrome *c* oxidase from *Paracoccus denitrificans*. *Nature* **376,** 660–669 (1995).
8. Kuriyan, J. *et al*. Convergent evolution of similar function in two structurally divergent enzymes. *Nature* **352,** 172–174 (1991).
9. Holm, L. & Sander, C. Mapping the protein universe. *Science* **273,** 595–602 (1996).
10. Mattevi, A. *et al*. Structure of L-aspartate oxidase: implications for the succinate dehydrogenase/fumarate reductase oxidoreductase family. *Structure* **7,** 745–756 (1999).
11. Singer, T. P. & McIntire, W. S. Covalent attachment of flavin to flavoproteins: Occurrence, assay, and synthesis. *Methods Enzymol.* **106,** 369–378 (1984).
12. Cole, S. T., Condon, C., Lemire, B. D. & Weiner, J. H. Molecular biology, biochemistry and bioenergetics of fumarate reductase, a complex membrane-bound iron-sulfur flavoenzyme of *Escherichia coli*. *Biochim. Biophys. Acta* **811,** 381–403 (1985).
13. Kenny, W. C. & Kröger, A. The covalently bound flavin of *Vibrio succinogenes* succinate dehydrogenase. *FEBS Lett.* **73,** 239–243 (1977).
14. van Hellemond, J. J. & Tielens, A. G. M. Expression and functional properties of fumarate reductase. *Biochem. J.* **304,** 321–331 (1994).
15. Schröder, I. *et al*. Identification of active site residues of *Escherichia coli* fumarate reductase by site-directed mutagenesis. *J. Biol. Chem.* **266,** 13572–13579 (1991).
16. Unden, G. & Kröger, A. An essential sulfhydryl group at the substrate binding site of the fumarate reductase of *Vibrio succinogenes*. *FEBS Lett.* **117,** 323–326 (1980).
17. Tomb, J.-F. *et al*. The complete genome sequence of the gastric pathogen *Helicobacter pylori*. *Nature* **388,** 539–547 (1997).
18. Flachmann, R. *et al*. Molecular biology of pyridine nucleotide biosynthesis in *Escherichia coli*. Cloning and characterization of quinolate synthesis genes nadA and nadB. *Eur. J. Biochem.* **175,** 221–228 (1988).
19. Vik, S. B. & Hatefi, Y. Possible occurrence and role of an essential histidyl residue in succinate dehydrogenase. *Proc. Natl Acad. Sci. USA* **78,** 6749–6753 (1981).
20. Tsukihara, T. *et al*. Structure of the [2Fe-2S] ferredoxin I from *Aphantothece sacrum* at 2.2 Ångstroms resolution. *J. Mol. Biol.* **216,** 399–410 (1990).
21. Körtner *et al. Wolinella succinogenes* fumarate reductase contains a dihaem cytochrome *b*. *Mol. Microbiol.* **4,** 855–860 (1990).
22. Hägerhäll, C. & Hederstedt, L. A structural model for the membrane-integral domain of succinate:quinone oxidoreductases. *FEBS Lett.* **389,** 25–31 (1996).
23. Simon, J. *et al*. Deletion and site-directed mutagenesis of the *Wolinella succinogenes* fumarate reductase operon. *Eur. J. Biochem.* **251,** 418–426 (1998).
24. Xia, D. *et al*. Crystal structure of the cytochrome *bc1* complex from bovine heart mitochondria. *Science* **277,** 60–66 (1997).
25. Unden, G., Albracht, S. P. J. & Kröger, A. Redox potentials and kinetic properties of fumarate reductase complex from *Vibrio succinogenes*. *Biochim. Biophys. Acta* **767,** 460–469 (1984).
26. Salerno, J. C. Electron transfer in succinate:ubiquinone reductase and quinol:fumarate reductase. *Biochem. Soc. Trans.* **19,** 599–605 (1991).
27. Lancaster, C. R. D. Quinone-binding sites in membrane proteins: what can we learn from the *Rhodopseudomonas viridis* reaction centre? *Biochem. Soc. Trans.* **27,** 591–596 (1999).
28. Hederstedt, L. Bioenergetics—Respiration without O_2. *Science* **284,** 1941–1942 (1999).
29. Bronder, M., Mell, H., Stupperich, E. & Kröger, A. Biosynthetic pathways of *Vibrio succinogenes* growing with fumarate as terminal electron acceptor and sole carbon source. *Arch. Microbiol.* **131,** 213–223 (1982).
30. Unden, G., Hackenberg, H. & Kröger, A. Isolation and functional aspects of the fumarate reductase involved in the phosphorylative electron transport of *Vibrio succinogenes*. *Biochim. Biophys. Acta* **591,** 275–288 (1980).
31. Tsiotis, G. in *A Practical Guide to Membrane Protein Purification* (eds von Jagow, G. & Schägger, H.) 149–159 (Academic, San Diego, 1994).
32. McPherson, A. *Crystallization of Biological Macromolecules* 304–305 (Cold Spring Harbor Laboratory Press, Cold Spring Harbor, 1999).
33. Otwinowski, Z. & Minor, W. Processing of X-ray diffraction data collected in oscillation mode. *Methods Enzymol.* **276,** 307–326 (1997).
34. Collaborative Computation Project, Number 4. The CCP4 suite: programs for protein crystallography. *Acta Crystallogr. D* **50,** 760–763 (1994).
35. De La Fortelle, E. & Bricogne, G. Maximum-likelihood heavy-atom parameter refinement for multiple isomorphous replacement and multiwavelength anomalous diffraction methods. *Methods Enzymol.* **276,** 472–494 (1997).
36. Otwinowski, Z. in *Proc. CCP4 Study Weekend, 25-26 Jan 1991, Isomorphous Replacement and Anomalous Scattering* (eds Wolf, W., Evans, P. R. & Leslie, A. G. W.) 80–86 (SERC Daresbury Laboratory, Warrington, UK, 1991).
37. Cowtan, K. dm: An automated procedure for phase improvement by density modification. *Joint CCP4 and ESF-EACBM Newsletter on Protein Crystallography* **30,** 34–38 (1994).
38. Jones, T. A., Zou, J. Y., Cowan, S. W. & Kjeldgaard, M. Improved methods for building protein models in electron density maps and the location of errors within these models. *Acta Crystallogr. A* **47,** 110–119 (1991).
39. Brünger, A. T. *et al*. Crystallography and NMR system: A new software suite for macromolecular structure determination. *Acta Crystallogr. D* **54,** 905–921 (1998).
40. Brünger, A. T. Free *R* value: a novel statistical quantity for assessing the accuracy of crystal structures. *Nature* **355,** 472–475 (1992).
41. Kleywegt, G. J. & Brünger, A. T. Checking your imagination: Applications of the free *R* value. *Structure* **4,** 897–904 (1996).
42. Luzzati, P. V. Traitement statistique des erreurs dans la détermination des structures cristallines. *Acta Crystallogr.* **5,** 802–810 (1952).
43. Read, R. J. Improved Fourier coefficients for maps using phases from partial structures with errors. *Acta Crystallogr. A* **42,** 140–149 (1986).
44. Engh, R. H. & Huber, R. Accurate bond and angle parameters for X-ray protein structure refinement. *Acta Crystallogr. A* **47,** 392–400 (1991).
45. Lancaster, C. R. D. & Michel, H. The coupling of light-induced electron transfer and proton uptake as derived from crystal structures of reaction centres from *Rhodopseudomonas viridis* modified at the binding site of the secondary quinone, Q_B. *Structure* **5,** 1339–1359 (1997).
46. Kraulis, P. J. MolScript: a program to produce both detailed and schematic plots of protein structures. *J. Appl. Crystallogr.* **24,** 946–950 (1991).
47. Esnouf, R. M. An extensively modified version of MolScript that includes greatly enhanced coloring capabilities. *J. Mol. Graphics Mod.* **15,** 132–134 (1997).
48. Esnouf, R. M. Further additions to MolScript version 1.4, including reading and contouring of electron-density maps. *Acta Crystallogr. D* **55,** 938–940 (1999).
49. Kabsch, W. & Sander, C. Dictionary of protein secondary structure: Pattern recognition of hydrogen-bonded and geometrical features. *Biopolymers* **22,** 2577–2637 (1983).
50. Merritt, E. A. & Bacon, D. J. Raster3D: Photorealistic molecular graphics. *Methods Enzymol.* **277,** 505–524 (1997).

Supplementary information is available at *Nature*'s World-Wide Web site (http://www.nature.com) or as paper copy from the London editorial office of *Nature*.

Acknowledgements

We thank A. Mattevi and co-workers for providing the coordinates of the *E. coli* L-aspartate oxidase before release for the Protein Data Bank; S. Gemeinhardt, O. Schürmann (both Institut für Mikrobiologie), C. Weiss, B. Marx, C. Münke, C. Wardenberg and D. Vinzenz (all at MPI Biophysik) for technical assistance; A. Thompson (EMBL Grenoble), G. Leonard and E. Mitchell (both ESRF) for support during data acquisition and preliminary data processing at ESRF Grenoble beamline BM14; and L.-O. Essen for providing purified tetrakis-(acetoxymercuri)-methane (TAMM). This work was supported by the Deutsche Forschungsgemeinschaft (SFB 472, grants to A.K. and H.M.) and the Max-Planck-Gesellschaft.

Correspondence and requests for materials should be addressed to C.R.D. L. (e-mail: lancaster@mpibp-frankfurt.mpg.de) and H.M. (e-mail: michel@mpibp-frankfurt.mpg.de). Atomic coordinates of the structures for both crystal forms have been deposited in the Protein Data Bank (accession codes 1QLA (form A) and 1QLB (form B)).